

Machine learning for accuracy in density functional approximations

Johannes Voss^{*†}

November 2, 2023

Abstract

Machine learning techniques have found their way into computational chemistry as indispensable tools to accelerate atomistic simulations and materials design. In addition, machine learning approaches hold the potential to boost the predictive power of computationally efficient electronic structure methods, such as density functional theory, to chemical accuracy and to correct for fundamental errors in density functional approaches. Here, recent progress in applying machine learning to improve the accuracy of density functional and related approximations is reviewed. Promises and challenges in devising machine learning models transferable between different chemistries and materials classes are discussed with the help of examples applying promising models to systems far outside their training sets.

Keywords: Machine learning, density functional theory, materials prediction, exchange-correlation functional, self-interaction, electron delocalization ■

^{*}SUNCAT Center for Interface Science and Catalysis, SLAC National Accelerator Laboratory, 2575 Sand Hill Road, Menlo Park, CA 94025, USA

[†]vossj@slac.stanford.edu

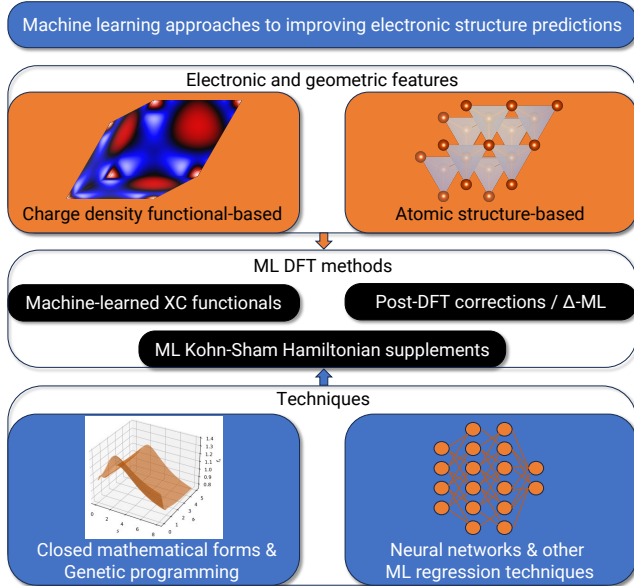


Figure 1: Overview of ML approaches to increasing the accuracy of electronic structure predictions based on electronic or atomic structural features. Machine-learned XC functionals are trained on high-accuracy benchmark data to improve upon the predictive power of existing DFAs. Post-DFT and Δ -ML methods provide improved energetics on fixed DFT charge densities, and other ML approaches supplement the Kohn-Sham Hamiltonian with Hubbard and dispersion terms.

1 INTRODUCTION

Machine learning (ML) techniques play an increasingly important role in atomistic-scale simulations in computational chemistry and physics.¹⁻³ Major areas of research are the acceleration of materials discovery and extending computationally accessible time and length scales through accelerated simulations. Inter-atomic potentials represented by neural networks⁴⁻⁷ or other ML regression techniques^{8,9} enable accurate molecular dynamics simulations for system sizes and time scales well beyond what can be achieved with first-principles Hamiltonians.¹⁰ When computation of the Born-Oppenheimer potential energy surface is not required, ML approaches trained to map chemical composition and other not necessarily atomic structure sensitive features to system properties of interest are powerful methods for direct, approximate materials property predictions.¹¹⁻¹⁵ Such methods can furthermore be employed for inverse materials design, where molecules or materials compositions that could lead to a desired target metric are predicted.^{16,17} These models and inter-atomic potentials are trained on high-throughput datasets generated with computationally affordable methods. Density functional theory (DFT)¹⁸ is often the method of choice due to a favorable trade-off between computational complexity and accuracy for the prediction of the electronic structures of molecules and solids.^{19,20} Some (minor or appreciable) loss in accuracy with respect to the DFT training data is typically tolerated with the advantage of significant speed up of the resulting ML methods over DFT simulations. At best, these ML methods can reproduce the quality of the DFT training data.

ML approaches are, however, also employed to increase the accuracy of DFT and related methods rather than substituting these first-principles approaches completely with ML models for acceleration. The ML methods are trained against chemically accurate quantum chemistry reference data or experimental benchmark data, where sufficient accuracy with beyond-DFT methods currently cannot be achieved. These methods can be categorized (Figure 1) into machine-learned density functionals for exchange and correlation (XC), atomic structure-dependent, machine-learned Hamiltonian corrections, and Δ -ML approaches that learn a correction to be applied to DFT results (as post-DFT corrections), with some methods belonging to more than one of these categories. Here, recent progress in ML approaches to increasing accuracy and to correcting fundamental errors in density functional approximations (DFA) is reviewed. These approaches hold the promise of providing DFT predictions with chemical accuracy and enabling accurate electronic structure simulations where DFAs fundamentally fail and which are currently out of reach for higher levels of theory. There are, however, challenges in availability of accurate training data for these latter systems and there can be issues with transferability of the ML methods beyond their training data. Examples are provided demonstrating such transferability issues for promising ML models.

2 SHORTCOMINGS OF DENSITY FUNCTIONAL APPROXIMATIONS

DFT drastically reduces the complexity of the electronic structure problem by expressing the total energy E_{total} of a system as a functional of the electronic charge density ρ rather than the many-electron wave function. In the Kohn-Sham (KS) formulation of DFT, this density functional is

$$E_{\text{total}}[\rho] = T_{\text{KS}}[\rho] + E_{\text{XC}}[\rho] + E_{\text{H}}[\rho] + E_{\text{ext}}[\rho]. \quad (1)$$

$T_{\text{KS}}[\rho]$ is the kinetic energy of an auxiliary system of non-interacting particles with the same density ρ as the true system of interacting electrons. Functional differentiation $\delta E_{\text{total}}/\delta\rho$ leads to a set of single-particle like KS equations with an effective one-body KS potential, from which $T_{\text{KS}}[\rho]$ is computed. $E_{\text{ext}}[\rho]$ accounts for the interaction with an external potential (given, *e.g.*, by interaction with nuclei) and $E_{\text{H}}[\rho]$ for the electrostatic interaction of the density with itself. The XC functional $E_{\text{XC}}[\rho]$ accounts for the two-body Coulomb interaction of the electrons and corrects for self-interaction in $E_{\text{H}}[\rho]$ and differences between $T_{\text{KS}}[\rho]$ and the kinetic energy of interacting electrons. In principle, Eq. 1 is exact, was $E_{\text{XC}}[\rho]$ known. In practice, $E_{\text{XC}}[\rho]$ must be approximated.

A few of the issues of approximations to $E_{\text{XC}}[\rho]$, some of which could be improved upon using ML methods, are summarized below. For a review of the limitations of DFAs, the reader is referred to Refs. [21–25].

The exact (unknown) $E_{\text{XC}}[\rho]$ is a universal functional not depending on the system in consideration. Approximations to it typically perform better for prediction of some materials properties at the cost of a worse prediction of others. Generalized gradient approximations (GGA), in which $E_{\text{XC}}[\rho]$ is expressed locally as a functional of the density and its gradient, improve upon the simplest approximation only depending on the local density (local

density approximation: LDA; local spin density approximation: LSDA), which is fitted accurately^{26,27} against Quantum Monte Carlo (QMC) simulations of the homogeneous electron liquid.²⁸ Some GGAs perform relatively well for solid structural and elastic properties but not for reaction energetics and vice versa.^{29–32} Meta-GGAs, that additionally dependent on the Kohn-Sham kinetic energy density τ or the Laplacian of ρ improve the range of applicability over GGA approaches.^{33–38}

The spurious electrostatic interaction of an electron with itself contained in the Hartree term E_H is difficult to compensate with the above semi-local functionals in strongly inhomogeneous systems or systems with localized states due to the long range of Coulomb interactions. One consequence of this inherent difficulty is spurious charge transfer across inter atomic separations at which the interaction between the separated subsystems should have vanished leading to neutral atoms. Hartree-Fock (HF) exchange exactly cancels this type of self-interaction error, and hybrid functionals combine semi-local DFT with (some amount of) such exact exchange (EXX) energies (at increased computational cost over semi-local DFT).³⁹ Range-separated hybrids consider screened exchange integrals, retaining EXX only at short or long range. Long-range EXX^{40,41} is required to cancel the long-range Hartree self-interaction. Metallic systems, on the other hand, are incorrectly described by long-range EXX with a vanishing density of states at the Fermi level. Metals are thus studied with short-range hybrids,⁴² which unfortunately do not cancel the long-range part of the Hartree self-interaction. These conflicting requirements for short *vs.* long-range EXX make it particularly difficult to accurately model the interaction of molecules with metallic surfaces with hybrid DFT.⁴³ One-electron self-interaction errors can generally be addressed with the self-interaction correction scheme by Perdew and Zunger,²⁷ improving, *e.g.*, charge transfer energetics and the description of negative ions. The prediction of thermochemistry is, however, worsened over uncorrected DFAs,⁴⁴ and also equilibrium geometries of molecules and solids are not systematically improved.⁴⁵

Even for gapped systems that can be studied with long-range hybrids, fundamental problems in the predicted electronic structures can exist in the presence of strong static correlation. Since the auxiliary KS system is composed of non-interacting particles, T_{KS} is computed from a single Slater determinant of KS orbitals. While the exact $E_{XC}[\rho]$ could compensate for the difference to the true, interacting electronic kinetic energy with significant multi-determinantal contributions (unless the true ground state density should turn out to not be representable by a non-interacting system with local KS effective potential²¹), approximations to $E_{XC}[\rho]$ typically lead to significant qualitative errors in *e.g.* predicting the energetics of multiradical molecules.⁴⁶ While KS spin-orbital occupation-constrained DFT can be used to compute corrections to some of these static correlation errors,^{47,48} in the general case of molecular interactions or molecule-metal interaction, where such constraints cannot be straightforwardly or uniquely defined or applied, static correlation is a fundamental problem for DFT and hybrid DFT. Long-range hybrids plus orbital-dependent random phase approximation⁴⁹ (RPA) correlation were shown to improve upon the description of strong static correlation in the dissociation limit of singly positively charged dimers.⁵⁰

Another shortcoming of DFAs is the incorrect prediction of total energies as a function of number of electrons N . Fractional values of N correspond to quantum mechanical ensemble averages of systems with different integer electron counts. Between adjacent integer values of N , the total energy scales linearly with N with derivative discontinuities at integer N .⁵¹

Semi-local DFAs do not reproduce the linear behavior nor the derivative discontinuities but rather show a convex behavior of $E_{\text{total}}(N)$, thus predicting too low energies for fractional N corresponding to a delocalization error favoring overly delocalized charge distributions over more localized ones with integer occupations.⁵² Supplementing the KS Hamiltonian with Hubbard terms in DFT+ U approaches^{53–55} canceling⁵⁶ the spurious curvature of $E_{\text{total}}(N)$ fundamentally improves the description of systems with strong d -electron or f -electron localization, such as several insulating transition-metal oxides and lanthanides and actinides, respectively. Predicting chemical reaction energies with DFT+ U approaches is, however, difficult, as only total energies with same Hubbard U -parameters for each ion in products *vs.* reactants can be compared directly. Transition-metal oxide formation energies computed with average, empirical U -parameters applied both to oxides and metals are an improvement over GGA predictions,⁵⁷ at the prize of a worse description of the bandstructure of metallic phases.⁵⁸ The lack of the derivative discontinuity and resulting delocalization error for semi-local DFAs furthermore can be used to explain the DFA band gap problem of generally underestimating the band gaps of semiconductors and insulators.⁵⁹ Orbital-dependent DFAs were constructed to provide derivative discontinuity corrections that added to KS band gaps approximately yield the desired fundamental gaps.⁶⁰

Semi-local DFAs fail at describing van der Waals (vdW) interactions. Here, density-density convolution approaches^{61–63} provide nonlocal DFA corrections which are quite successful in describing dispersion forces. Alternatively, force fields (with fixed or density-dependent dispersion coefficients) can correct the potential energy surfaces computed with semi-local DFAs by vdW interactions.^{64–68}

For molecular systems of sufficiently low electron count N , there are wave function-based quantum chemistry methods, which can provide accurate electronic structures, not suffering from the above problems of DFAs. For extended systems, in particular those involving metallic states, obtaining results more accurate than those from semi-local DFAs is difficult, and experiments often serve as the benchmark for DFAs. In the following section, reference data that can serve for training electronic structure ML models are summarized.

3 GROUND TRUTH FOR DFA ML MODELS

3.1 Thermochemistry, thermochemical kinetics, and molecular interactions

Experimental data for heats of formation of molecules are common benchmarks for DFAs and quantum chemistry (*i.e.* generally wave function-based) methods. The ‘‘Gaussian- n ’’ theories of composite quantum chemistry techniques,^{69,70} *e.g.*, were benchmarked against experimental data on heats of formation, ionization potentials, electron affinities, and proton affinities, with ~ 1 kcal/mol errors.^{71,72} Having thus established chemical accuracy of the approaches for these molecular properties, further accurate training and benchmark data for DFAs and ML models can be computed in high throughput with these quantum chemistry methods. Ramakrishnan *et al.*⁷³ used the Gaussian-4-Møller-Plesset-2 level of theory⁷⁴ to compute the heats of formation of over 100,000 molecules constituting the QM9 dataset (out of $\sim 2 \cdot 10^{11}$ molecules enumerated in the GDB-17 dataset⁷⁵). Using the Weizmann-4 quantum

chemistry protocol,^{76,77} Karton *et al.* were able to compute training targets for atomization energies of 140 molecules and radicals in the W4-11 dataset⁷⁸ and of 200 molecules and radicals in the W4-17 dataset⁷⁹ with estimated accuracies better than 1 kcal/mol, also providing computed zero-point energies.

Řezáč *et al.*^{80,81} computed the non-covalent interaction energies of 66 molecular complexes at 8 inter-molecular separations using coupled cluster theory⁸² with triple excitations and complete basis set limit extrapolation. These S66/S66x8 datasets (later revised by Brauer *et al.*⁸³) are particularly useful for parameterizing or training approaches to describe dispersion energetics and forces.

Gas phase reaction barrier height benchmarks were established by combining several quantum chemistry approaches and experimental results by Zheng *et al.*^{84,85} in the DBH24 dataset and by Zhao *et al.*^{86,87} in the BH-76 dataset. These two barrier height and other datasets are included in the GMTKN55 dataset by Goerigk *et al.*,⁸⁸ which is a collection of datasets for thermochemistry, thermochemical kinetics, and non-covalent interactions. A further aggregate molecular chemistry benchmark dataset was compiled by Mardirossian and Head-Gordon.⁸⁹ Chan *et al.*⁹⁰ collected quantum chemistry benchmark data for transition-metal (complex) chemistry in the TMC151 dataset.

For heats of formation of solids, the tables of Kubaschewski *et al.*⁹¹ provide a wide range of experimental data. These data were *e.g.* used to parameterize empirical schemes to combine DFT+ U energetics for correlated transition-metal oxides with DFT for metallic phases in the Materials Project.^{92,93} Kirklin *et al.*⁹⁴ have collected experimental solid formation energies for benchmarking their Open Quantum Materials Database of GGA simulations of solids. For solid cohesive energies, experimental data collected in Refs. [95,96] was combined in the CE65 dataset, where zero-point contributions estimated from experimental Debye temperatures and DFT phonon calculations (neglecting minor dependencies of phonon frequencies for these solids on the choice of a solid state-appropriate GGA) were subtracted from the experimental cohesive energies as total solid atomization energy training targets.³⁷

3.2 Atomic structures

The above-described thermochemistry datasets QM9, W4-11, and W4-17 also provide optimized equilibrium geometries of the considered molecules and radicals. Staroverov *et al.*⁹⁷ employed Gaussian-3X theory⁹⁸ to determine the equilibrium bond lengths of 86 neutral molecules and 10 molecular cations (forming the T-96R dataset), and the equilibrium structures and vibrational frequencies for 69 neutral and 23 cation dimers (forming the T-82F dataset). These data can be used to train models to yield accurate equilibrium molecular geometries and harmonic vibrational properties.

For solids, the currently used benchmark and training data for structures are, as is the case for thermochemistry, based on experimental data with zero-point contributions removed from lattice constants and bulk moduli according to GGA phonon calculations or experimental Debye temperatures. Alchagirov *et al.*⁹⁹ used the latter approach entirely based on experimental data in a Debye model to remove zero-point contributions from the observed lattice constants and bulk moduli of 17 solids. Hao *et al.*¹⁰⁰ computed the phonon frequencies of 58 cubic solids using the PBE GGA¹⁰¹ to remove zero-point contributions from the experimental lattice constants. Trepte *et al.*¹⁰² similarly used PBE phonon calculations

by Zhang *et al.*⁹⁶ to subtract zero-point contributions from the experimental bulk moduli of 62 solids as training target for ML DFA models. The advantage of removing zero-point contributions from the experimental lattice and elastic data is that the DFA training can directly minimize the error on these properties with few total energy predictions without also having to predict the computationally more costly phonon frequencies during training.

3.3 Transition-metal surface chemistry

Transition-metal surface chemistry constitutes an interesting challenge for DFAs, as spurious charge transfer problems between surface and adsorbates can occur and molecules can exhibit strong static correlation, while the metallic surface bandstructure requires a good description of metallic screening. Experimental results for 39 chemi- and physisorption energies on transition-metal surfaces were collected by Wellendorff *et al.*¹⁰³ and PBE zero-point contributions to be removed from the experimental results for DFA training were computed. These data were extended by one chemi- and one physisorption energy resulting in the ADS41 dataset.⁴³

Surface reaction barrier heights pose the additional challenge of delocalization errors in transition state geometries for DFAs. Mallikarjun Sharada *et al.*¹⁰⁴ collected ten measured surface barrier heights for molecular dissociation on transition-metal surfaces forming the SBH10 dataset. This dataset was extended by Tchakoua *et al.*¹⁰⁵ by 7 more surface reaction barrier heights resulting in the SBH17 dataset.

These surface chemistry data are computationally more expensive to train ML DFA models against than the bulk solid data above. The considered bulk systems typically are cubic and highly symmetric, such that the lattice constant is the only structural degree of freedom to be optimized to predict equilibrium structures. For surface and adsorbate systems, nuclear coordinate degrees of freedom for surface and adsorbate atoms need to be relaxed, too, and the slab models typically contain on the order of 20 transition-metal atoms, thus rendering each total energy calculation significantly more expensive than in the small primitive unit cell bulk cases. These surface chemistry benchmarks from single-crystal experiments are, however, very valuable as their simulation requires accurate description of both extended and localized states and their interactions.

3.4 Charge densities

Medvedev *et al.*¹⁰⁶ have benchmarked DFAs for their prediction of molecular charge densities compared to accurate quantum chemistry densities, finding that while newly developed DFAs have become better at predicting energies, the prediction of densities has been sacrificed to some degree. Quantum chemistry charge densities are thus an important training target for accurate ML DFAs. ML efforts reviewed in the following that consider such density metrics during their training typically computed quantum chemistry densities as part of the studies, with public quantum chemistry charge density benchmark data (rather than DFT densities) being hard to find.

4 ML XC FUNCTIONALS

We divide ML DFAs into two categories. The first category summarized in the following consists of density functionals represented by mathematical expressions of explicit, tractable functional form with a low to moderate number of fitted numerical coefficients. The second category consists of functionals represented by neural networks with linear, convolutional, and non-linear activation layers,¹⁰⁷ where the neural network weights typically constitute a much larger space of fitting degrees of freedom than the coefficients in the former explicit density functionals forms.

4.1 Semi-empirical DFAs with explicit functional forms

A major (and lasting) impact on the adoption of GGAs for computational chemistry had the development of semi-empirical DFAs fitted against thermochemistry by Becke (followed a few years later by the non-empirical PBE¹⁰¹ functional and its lasting impact on computational materials science). In Becke’s hybrid DFA B3PW91,¹⁰⁸ relative weights for exact, local, semi-local exchange and local and semi-local correlation were fitted against the G2 thermochemistry dataset¹⁰⁹ (the popular B3LYP functional replaces PW91¹¹⁰ correlation with LYP¹¹¹ correlation¹¹²; Vargas-Hernández¹¹³ employed Bayesian optimization¹¹⁴ to choose the weighted exchange and correlation functionals and to optimize the weights). In Becke’s B97 hybrid,¹¹⁵ exchange and correlation inhomogeneity correction factors were introduced. These factors are polynomials in fractions of the reduced density gradient $\sim |\nabla\rho|/\rho^{4/3}$, and the polynomial coefficients were also fitted against the G2 dataset. Mardirossian and Head-Gordon¹¹⁶ extended this work to a long-range screened hybrid and nonlocal correlation, ω B97X-V, identifying which powers led to the best fit to a wider range of molecular benchmark data, also optimizing the empirical coefficients of the used VV10 nonlocal correlation functional,⁶³ and eliminating a few fitting degrees with constraints. Liu *et al.*¹¹⁷ fitted a meta-hybrid with nonlocal correlation functional on a wide range of molecular chemistry benchmarks including thermochemistry, barrier heights, isomerization energies, excitation energies, non-covalent interactions, dipole moments, and bondlengths.

Following the strategy of fitting polynomial coefficients to molecular thermochemistry, Hamprecht *et al.*¹¹⁸ optimized inhomogeneity correction factors for a GGA with a small increase in number of polynomial coefficients compared to the Becke functionals, starting the development of the HCTH-family of XC functionals.^{119–121} Truhlar and co-workers developed the semi-empirical Minnesota XC functionals, which includes meta-GGAs and hybrid meta-GGAs.^{122–127} During the development of this XC functional family, the range of training data was widened, including solid properties in addition to molecular chemistry. In some of the Minnesota functionals, analytical constraints were used to reduce the large number (up to over 50) of fitting degrees of freedom.¹²⁸

The performance of the strongly constrained and appropriately normed (SCAN) meta-GGA³⁴ clearly showed the benefits of fulfilling an increasing number of known analytical constraints for XC functionals.^{129,130} Sparrow *et al.*¹³¹ expressed inhomogeneity factors for GGA exchange and correlation in a spline basis facilitating straightforward enforcement of equality and inequality constraints, resulting in the CASE21 functional for molecular chemistry. In addition to coefficient elimination for equality constraints, inequality constraints

were implemented as penalties during exchange enhancement factor optimization of the meta-GGA MCML by Brown *et al.*³⁷ for bulk, surface, and gas-phase chemistry. This constrained meta-GGA optimization was extended by Trepte *et al.*¹⁰² to a simultaneously optimized, nonlocal VV10⁶³ correlation term.

Rather than imposing analytical constraints, overfitting in the Bayesian error estimation functionals (BEEF) was suppressed by a quadratic (Tikhonov¹³²) regularizer.^{95,133,134} This ridge regression approach¹³⁵ led to a fast decay of the magnitude of polynomial coefficients with increasing polynomial powers in the series used to expand the GGA and meta-GGA exchange enhancement factors. In contrast to many non- and semi-empirical XC functionals, the BEEF functionals enhance exchange for a homogeneous system over the exact local exchange in this limit. Similar exchange enhancement increase in the homogeneous limit by a few percent was also observed by Kovács *et al.*¹³⁶ for meta-GGA exchange enhancement fits to lattice constants, solid cohesive energies, and band gaps when not imposing this LDA limit.

Generally, the XC functional fitting approaches have evolved into using generic forms of enhancement or inhomogeneity factors with a large number of fitting degrees of freedom. Gastegger *et al.*¹³⁷ instead applied the ML technique of genetic programming¹³⁸ to find mathematically simple forms of XC functionals performing well for molecular chemistry benchmarks. Ma *et al.*¹³⁹ used similar symbolic regression techniques (by means of regularized evolution¹⁴⁰) to evolve generations of XC functionals starting from preexisting ones to new ones with improved performance on target datasets.

The above-reviewed semi-empirical XC functionals are optimized to yield quantitatively improved performance for desired chemistry target metrics. Fundamental DFA issues of the different levels of theory of hybrids, GGAs, and meta-GGAs are generally unlikely improved upon qualitatively by numerical optimization of these mathematically relatively simple XC functionals. Much more complex DFAs, such as neural network-based approaches reviewed below, might offer an opportunity to arrive at such qualitative improvement. Accurate, but system or materials class-specific functionals could also be learned with simpler ML models. Riemelmoser *et al.*¹⁴¹ used Gaussian kernel regression with nonlocal density features to learn ML functionals reproducing RPA correlation energies for diamond and water, respectively.

4.2 Neural network DFAs

Neural network XC functionals are functionals of density, density gradient and additional local electronic properties, such as KS kinetic and EXX energy densities, and are trained to yield accurate target XC energies and typically also accurate ground state densities (Figure 2). The automatic differentiation-based backpropagation technique¹⁴² commonly used for optimizing the neural network weights for loss function minimization during training is here applied to also compute the gradient of the XC energy with respect to the local density and energy density inputs. These derivatives are required to compute the KS potential.

Nagai *et al.*¹⁴³ trained a neural network meta-GGA on the quantum chemistry densities and atomization energies of only the three molecules H₂O, NH₃, and NO. The neural network weights were optimized via simulated annealing by selfconsistently computing the ground state densities and energies of the three molecules and H, N, and O atoms for randomly perturbed weights. Remarkably, the resulting XC functional performs well and even

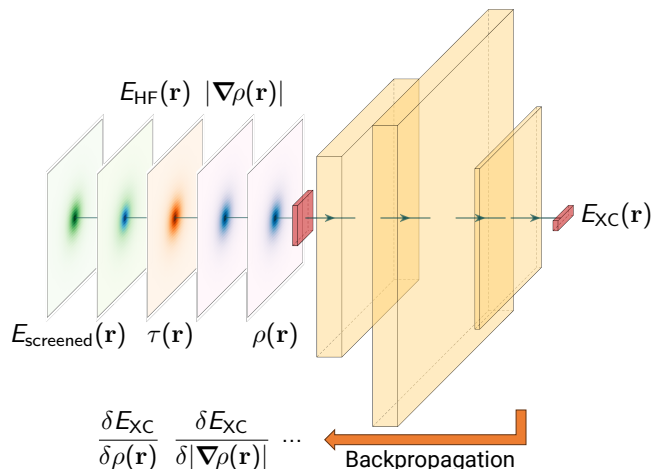


Figure 2: Schematic of a neural network-based XC functional. Local features of the charge density ρ at position \mathbf{r} and, depending on the XC functional type, kinetic (τ) or EXX energy densities are inputs to the neural network yielding the XC energy $E_{\text{XC}}(\mathbf{r})$. With the help of backpropagation, the gradient of the XC energy with respect to the inputs can be obtained, from which the effective one-body KS potential is computed.

outperforms existing functionals across benchmark databases containing over 100 molecules. The implied transferability from a very small training set to other molecules and also to reaction barriers is very promising. This neural network meta-GGA work was extended by enforcing five physical constraints on exchange and correlation each, and including the ionization potentials as an additional training target besides densities and atomization energies of the molecules H_2O , NH_3 , and CH_2 .¹⁴⁴ This XC functional was trained as an XC enhancement over the SCAN meta-GGA. While the resulting XC functional bares some similarity with the SCAN functional (Figure 3), it is reported to outperform SCAN on lattice constant and molecular atomization benchmarks.

Kirkpatrick *et al.*¹⁴⁵ developed a neural network XC functional addressing the total energy *vs.* fractional particle number and derivative discontinuity problem. Their DeepMind21 (DM21) functionals take point by point in real space charge density and gradient, KS kinetic, unscreened and long-range EXX energy densities as inputs. The training was performed non-selfconsistently on B3LYP densities and KS orbitals. The loss was computed as the energy differences to large sets of molecular chemistry benchmarks. The change in energy a single selfconsistent field iteration would cause starting from the B3LYP orbitals was estimated perturbatively for a subset of smaller systems, and this change was penalized as an additional term in the loss function. With this approach, the neural network weights could be optimized using the gradient obtained via backpropagation, as no KS selfconsistency cycles were required during training. This enabled training a relatively large neural network ($\sim 4 \cdot 10^5$ trainable weights) and on large datasets, which were extended by densities of fractional charges and spins to train the correct piece-wise linear behavior with energy *vs.* particle number derivative discontinuities. Energies and charge densities were interpolated linearly between integer particle numbers as dictated by quantum mechanical ensemble averages, spin densities were interpolated linearly between degenerate spin states, and the KS

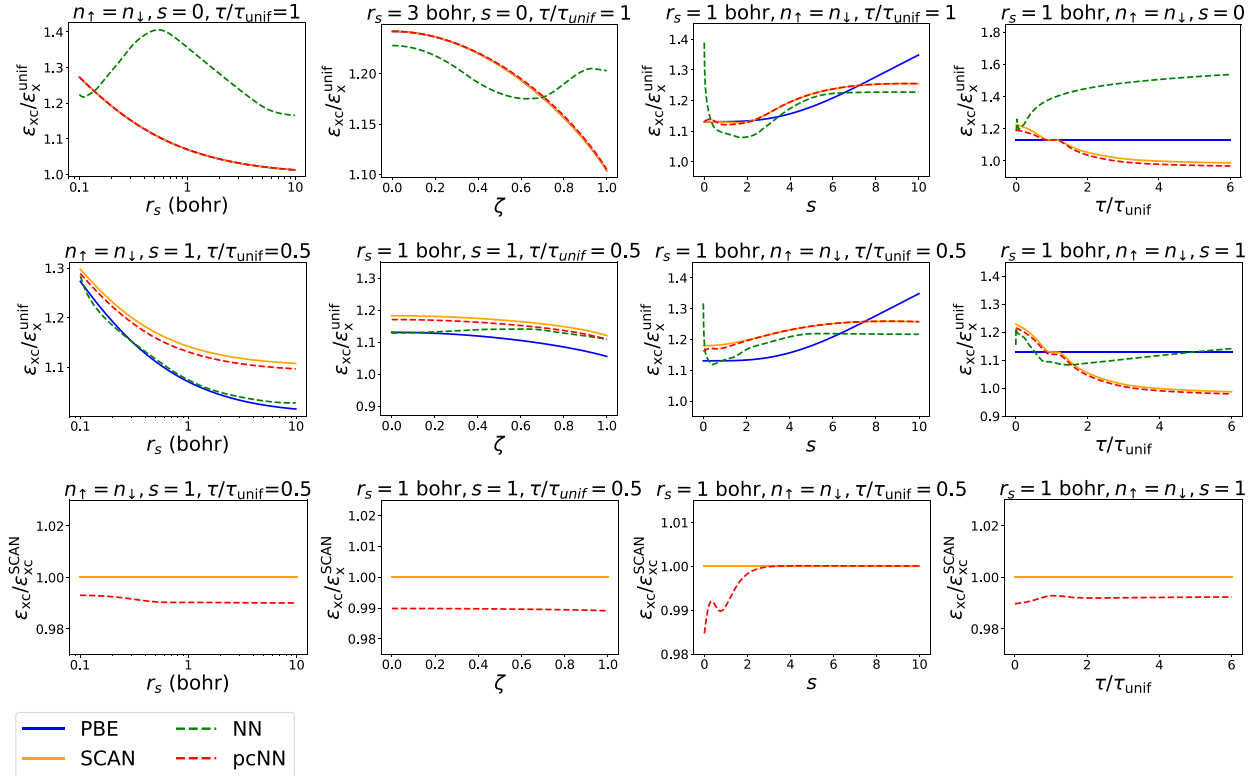


Figure 3: Comparison of the XC enhancement of the PBE,¹⁰¹ SCAN,³⁴ and neural network-based XC functionals without (NN) and with physical constraints (pcNN) for different values of Wigner-Seitz radius r_s , reduced density gradient s , KS kinetic energy density τ (relative to Thomas-Fermi kinetic energy density τ_{unif}), and relative spin polarization ζ . Two top rows: XC enhancement over local exchange ϵ_x^{unif} , bottom row: pcNN XC enhancement over SCAN XC functional. Reproduced from Ref. [144], DOI: [10.1103/PhysRevResearch.4.013106](https://doi.org/10.1103/PhysRevResearch.4.013106) under the terms of the Creative Commons Attribution 4.0 International License. Copyright 2022, the Authors. Published by the American Physical Society.

inversion technique due to Wu and Yang¹⁴⁶ was used to decompose the interpolated densities into KS orbitals for computation of the required DM21 input energy densities. Several variants of the DM21 functional were developed with different imposed constraints (fractional charge and spin constraints and homogeneous electron gas limit), showing promising performance on molecular benchmark data. Tests of two of these variants for solids, *i.e.*, materials classes outside the training data, are presented in the outlook at the end of this review.

Gedeon *et al.*¹⁴⁷ trained a neural network XC functional for correct derivative discontinuity behavior for 1D systems with the help of an additional neural network input feature explicitly depending on the total (fractional) particle number. Wang *et al.*¹⁴⁸ iteratively trained a neural network GGA by using backpropagation to optimize the neural network at fixed charge densities and then using this neural network GGA to recompute charge densities in KS selfconsistency cycles at fixed neural network weights. Chen *et al.*¹⁴⁹ similarly performed iterative loops of neural network optimization at fixed orbitals and KS solution

at fixed neural network weights for DFT and hybrid DFT.

Rather than employing the techniques in the above approaches to XC neural network optimization of simulated annealing, perturbative approaches, and iterative loops between neural network backpropagation-based optimization and KS selfconsistency cycles, there are efforts to make the KS solution with its challenge of required selfconsistency between KS orbitals and density differentiable. Li *et al.*¹⁵⁰ implemented a differentiable KS solution for 1D systems, which they trained on accurate solutions possible in this reduced dimensionality within the density matrix renormalization group (DMRG).¹⁵¹ Their loss function penalizes differences in the converged KS density and the DMRG one as well as the total energy difference at each KS iteration to the DMRG energy. This approach enhances the smooth convergence rate of the KS cycles towards the DMRG solution, with the KS equations effectively acting as a regularizer. The KS regularization helps the ML functional learn smooth functional derivatives not only at the converged solution, but along the KS convergence trajectory. The regularization was furthermore found to enhance the transferability of the XC functional.¹⁵² Kasim and Vinko¹⁵³ implemented differentiable KS solutions in three dimensions, and Kasim *et al.*¹⁵⁴ extended this work to a differentiable DFT and HF code. Starting from accurate ground state densities instead, Tozer *et al.*¹⁵⁵ used a neural network to model the XC potential derived from configuration-interaction densities of atoms and small molecules using the KS inversion technique by Zhao *et al.*¹⁵⁶ for finite systems.

5 Δ -ML CORRECTIONS TO DFT

The approaches reviewed in the previous section learn approximations to the XC functional $E_{\text{XC}}[\rho]$, and functional differentiation yields the effective one-body KS potential used to compute KS orbitals and thus KS kinetic energies, EXX integrals, and other orbital-dependent energies. Instead of using the KS potential from the machine-learned XC functional and correspondingly solving the KS equations selfconsistently, the Δ -ML methods reviewed here provide post-DFT and post-hybrid DFT corrections to $E_{\text{XC}}[\rho]$, where the ground state density ρ and KS orbitals are kept fixed at the solution from another XC functional.

A resulting simplification for such Δ -ML methods is that they need not provide functional derivatives, as one-body KS potentials are not computed. This enables the usage of non-differentiable ML approaches such as the decision tree ensemble method of gradient boosting.^{157,158} Wang *et al.*¹⁵⁹ used the popular gradient boosting implementation XGBoost¹⁶⁰ to learn a density and density gradient-dependent (*i.e.* GGA-type) XC functional to be evaluated non-selfconsistently on PBE charge densities. This functional provides an XC energy correction on top of PBE XC, which was trained to improve upon molecular thermochemistry benchmarks. Similarly, Bogojeski *et al.*¹⁶¹ used kernel ridge regression to train a model correcting selfconsistent PBE-based energies to coupled cluster results. This XC model takes nonlocal density features as input (a second kernel ridge regression model was developed to predict these density features from the atomic structure alone). They found these Δ -XC energy corrections could be regressed with lower errors than coupled cluster or DFT energies directly, constituting another advantage of Δ -ML corrections to XC energies.

Another family of approaches non-selfconsistently provides correlation energies post self-consistent DFT or HF. Margraf and Reuter¹⁶² developed a kernel-based approach using

nonlocal charge density features that provides non-selfconsistent correlation energies trained on quantum chemistry energies. Chen *et al.*¹⁶³ developed a neural network-based approach for post-HF correlation energies also trained on molecular quantum chemistry. They used the local one-body density matrix as model input and trained an ensemble of neural networks. Deviation in the ensemble was used as a model uncertainty estimate in an active learning approach to limit the number of computationally expensive quantum chemistry simulations for training data. Cheng *et al.*¹⁶⁴ used Gaussian process regression¹⁶⁵ to develop a post-HF model for correlation energies using the one-body density matrix. One-body density matrix-derived features were similarly used by Ng *et al.*¹⁶⁶ to train neural networks to predict post-HF correlation energies. Han *et al.*¹⁶⁷ devised a semi-local ML XC functional for post-HF correlation energies trained against Møller-Plesset-2¹⁶⁸ data. Their functional takes charge density and gradient, electronic kinetic energy, and a weighted sum of the occupied orbital densities as local input. For the latter sum, the orbitals were weighted reciprocally with the energy difference of the HF energy level of the occupied orbital to the virtual orbitals, in order to mimic the energy denominators in second order perturbation theory in this feature.

6 ATOMIC STRUCTURE-DEPENDENT XC CORRECTIONS

While the Δ -ML methods summarized in the previous section predict post-DFT and HF corrections based on electronic features, atomic structural information can be employed to parameterize such XC corrections, too. Ramakrishnan *et al.*¹⁶⁹ used kernel ridge regression to non-selfconsistently correct HF to Møller-Plesset-2 and coupled cluster results as well as Møller-Plesset-2 to coupled cluster. The corrections are expressed as sums over terms measuring atom by atom the similarity of two structures through kernel functions exponentially decaying with atomic coordinate distances.

The DFT+ U method constitutes an atomic structure-dependent XC correction, as the Hubbard terms in this method are used to penalize fractional occupation of local density matrices in the basis of, *e.g.*, correlated transition-metal or rare-earth site-centered atomic orbitals. Using genetic programming with experimental transition-metal oxide heats of formation as training data, Δ -ML models were found that featurizing local density matrices enable reaction energy predictions based on different levels of theory for products and reactants.⁵⁸ Localized states in the correlated oxides were treated at the DFT+ U level with site-dependent, first-principles U -parameters from linear-response theory, and delocalized states in the metallic phases were treated at the DFT level.

Empirical force fields are ubiquitously used to supplement semi-local DFAs with dispersion energetics. Proppe *et al.*¹⁷⁰ used Gaussian process regression featurizing the individual pairwise terms of such vdW force fields to arrive at improved agreement with coupled cluster results. Variance prediction was used to select systems for coupled cluster benchmark calculations in an active learning framework.

A non-selfconsistent Δ -ML approach with an atomic structure and charge density-dependent XC energy correction was developed by Dick and Fernandez-Serra.¹⁷¹ In this work, the selfconsistent DFT charge density was projected onto atom-centered basis functions, defined as spherical harmonics times a radial function confined to a spherical shell

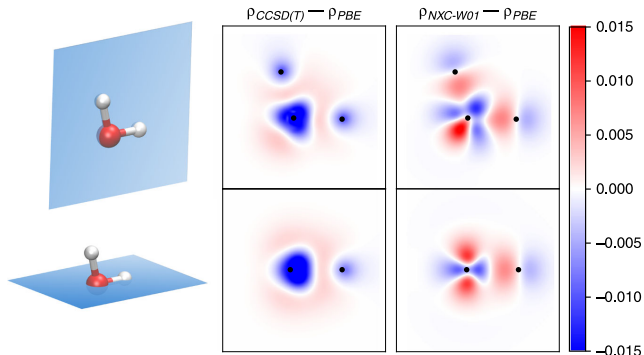


Figure 4: Comparison of water molecule charge density differences between coupled cluster theory and PBE (contour plots to the left) and between the NeuralXC functional and PBE (right). Reproduced from Ref. [174], DOI: 10.1038/s41467-020-17265-7 under the terms of the Creative Commons Attribution 4.0 International License. Copyright 2020, the Authors. Published by Springer Nature.

around the atom. In analogy to ML inter-atomic potentials, the Δ -XC energy correction was defined as a sum over atomic contributions, where each of these contributions is modeled by a neural network with the charge projections around the corresponding atom as input. As this non-selfconsistent Δ -ML approach does not provide corrections to the charge density, corrections to the atomic forces were trained with additional neural networks. The models were trained and tested on water clusters, for which in turn coupled cluster-based force field parameterizations^{172,173} were used as reference data.

Dick and Fernandez-Serra¹⁷⁴ extended this work to refined atom-projected density features that account for the charge density difference of the system to atomic reference densities, and they used backpropagation to compute derivatives with respect to these density features. They thus compute the functional derivative of their model with respect to the density resulting in an ML XC functional that can be used selfconsistently. Again benchmarking their model for water, they find, *e.g.*, an improved description of charge accumulation along the OH bonds compared to semi-local DFAs (Figure 4).

7 ML KS HAMILTONIAN SUBSTITUTIONS

ML approaches are not only used to find approximations to $E_{\text{XC}}[\rho]$, they can also be employed, *e.g.*, to approximate the non-interacting kinetic energy functional $T_{\text{KS}}[\rho]$ in Eq. 1. Such methods are not necessarily aimed at increasing the accuracy of DFT simulations, but typically rather at their acceleration. An explicit density-only functional for the non-interacting kinetic energy in KS orbital-free DFT would substantially reduce the computational cost of DFT, which for semi-local DFT with T_{KS} computed from KS orbitals is dominated by the diagonalization of the auxiliary Hamiltonian with KS one-body potential. Burke and coworkers developed neural network models for $T_{\text{KS}}[\rho]$ for 1D systems.^{175,176} Tan *et al.*¹⁷⁷ implemented a differentiable, orbital-free DFT code for efficient training of neural network-based approximations to $T_{\text{KS}}[\rho]$.

Finding that functional derivatives of neural network models of $T_{\text{KS}}[\rho]$ were typically

noisy and not generally useful for implementing a minimization scheme of the KS orbital-free energy functional (and regularization of the functional derivatives unfortunately correlated with a loss of accuracy of $T_{\text{KS}}[\rho]$ ¹⁷⁶), Brockherde *et al.*¹⁷⁸ machine-learned the map from external potential to ground state charge density instead of learning to approximate $T_{\text{KS}}[\rho]$. This approach absolves from a total energy functional minimization with respect to the density, and functional derivatives are thus not required. Given the promise of significantly improved computational efficiency of such an orbital-free DFT approach, further ML models directly predicting the charge density have been developed.^{179–184} Shao *et al.*¹⁸⁵ furthermore learned maps from external potential to the one-body density matrix.

Another avenue for electronic structure ML models targeting computational efficiency is the substitution of expensive energy contributions, such as EXX, with cheaper ML approximations. Cuierrier *et al.*¹⁸⁶ used a neural network to train a semi-local approximation of exchange exploiting the fourth order expansion of the exchange hole¹⁸⁷ as an input feature, where a relatively small neural network was optimized with a quasi-Newton approach. Their training target was EXX from hybrid DFT. Lei and Medford¹⁸⁸ trained a neural network to reproduce B3LYP XC with nonlocal density descriptors. Yu *et al.*¹⁸⁹ used Bayesian optimization to find Hubbard- U corrections that best reproduce the behavior of EXX in short-range screened hybrid DFT for solids. Bystrom and Kozinski¹⁹⁰ used Gaussian process regression to train an exchange functional reproducing EXX with a combination of semi-local and nonlocal density features. These approaches aim at reproducing the effects of EXX on the electronic structure at the cost of semi-local DFT.

8 CHALLENGES AND OPPORTUNITIES

The perhaps surprising usefulness of the simplest of DFAs, the LDA, even for inhomogeneous systems, was explained by XC energies only depending on the spherical average of the XC hole and the LDA fulfilling the important sum rule of this hole accounting for one missing electron.¹⁹¹ Density gradient corrections do not necessarily improve upon the predictive performance of the LDA, unless this sum rule is fulfilled. It was the real-space cut-off in the exchange hole gradient expansion introduced by Perdew¹⁹² that enabled the development of GGAs fulfilling the sum rule and outperforming the LDA for energetics and atomic structures. The success of the seemingly crude LDA and the reason for sum rule-fulfilling GGAs being able to outperform the LDA can thus be rationalized through physical understanding.

ML models, on the other hand, do not necessarily allow for such insights. Even with the simpler reviewed ML models with only a moderate number of fitting degrees of freedom, it cannot necessarily be excluded that the improvement over existing approaches merely consists of reducing error bars on the well-known benchmark data sets,¹⁹³ potentially at the price of *e.g.* sacrificing the description of the central quantity of DFT, the charge density, for improved reaction energy differences,¹⁰⁶ and thus potentially developing XC functionals that yield “right answers” for the “wrong reason”.¹⁹⁴ These empirical methods could show accidentally improved energetics with respect to some benchmarks without having led to improved physical approximation of electronic XC.

To highlight the promise that ML XC models hold, but also challenges in their transferability, we will compare here the performance of ML XC models to systems far outside their

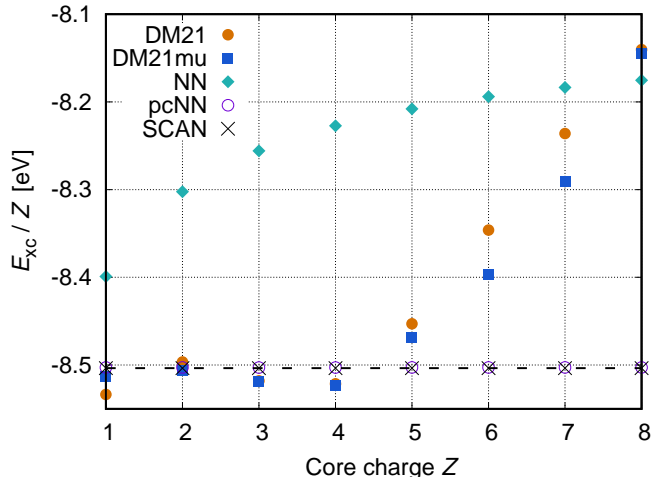


Figure 5: XC energies evaluated on the analytical exponential densities of hydrogenic ions as a function of the core charge Z . The dashed line marks the exact exchange energy of $-5/16 \text{ Hartree} \cdot Z$, which exactly cancels the spurious Hartree interaction in these one-electron systems.

training and validation data. We begin this discussion with a simple test of the XC models for their performance on hydrogenic ions (Figure 5). In these one-electron systems, accurate XC should exactly cancel the spurious one-electron Hartree interaction. The first neural network XC model (NN) by Nagai *et al.*,¹⁴³ only trained on three molecules but showing promising performance for a range of molecular thermochemistry, did not explicitly incorporate analytical constraints nor was it trained *e.g.* on the exact XC density of the H atom. Its performance for hydrogenic ions turns out to be relatively poor. The physically constrained pcNN¹⁴⁴ by the same authors, also only trained on three molecules, yields accurate XC energies for these ions. From the DM21 family of functionals, we consider the variant DM21 with fully imposed fractional charge and spin piece-wise linear energy behavior and the variant DM21mu with imposed homogeneous electron gas limit. Both DM21 and DM21mu show reasonable accuracy for hydrogenic ions with $Z < 5$, where the more positively charged ions are likely too far from the training data.

The derivative discontinuity trained for in the DM21 functional via fractional total charges on molecular systems is of importance for correcting KS gaps to the physical, fundamental gap of semiconductors and insulators. We thus test here the performance of DM21 functionals trained only on molecular data for a bulk system: the semiconductor Si (Figure 6). PBE, as is typical for DFAs, significantly underestimates the Si band gap. The DM21 functional shows poor performance for the Si bandstructure in general. The spurious oscillations in band dispersion as a function of wave vector are likely due to DM21 not being parameterized in the density and energy gradient neural network input tuples relevant for solids here. The bandstructure is overall compressed in energy range and with that the band gap, while one would have hoped that a functional reproducing derivative discontinuities would yield an enlarged band gap with respect to semi-local DFAs. DM21mu, on the other hand, yields a smooth band structure and an increased band gap in approximate agreement with experimental and GW ¹⁹⁵ results.¹⁹⁶ This is another example of the impor-

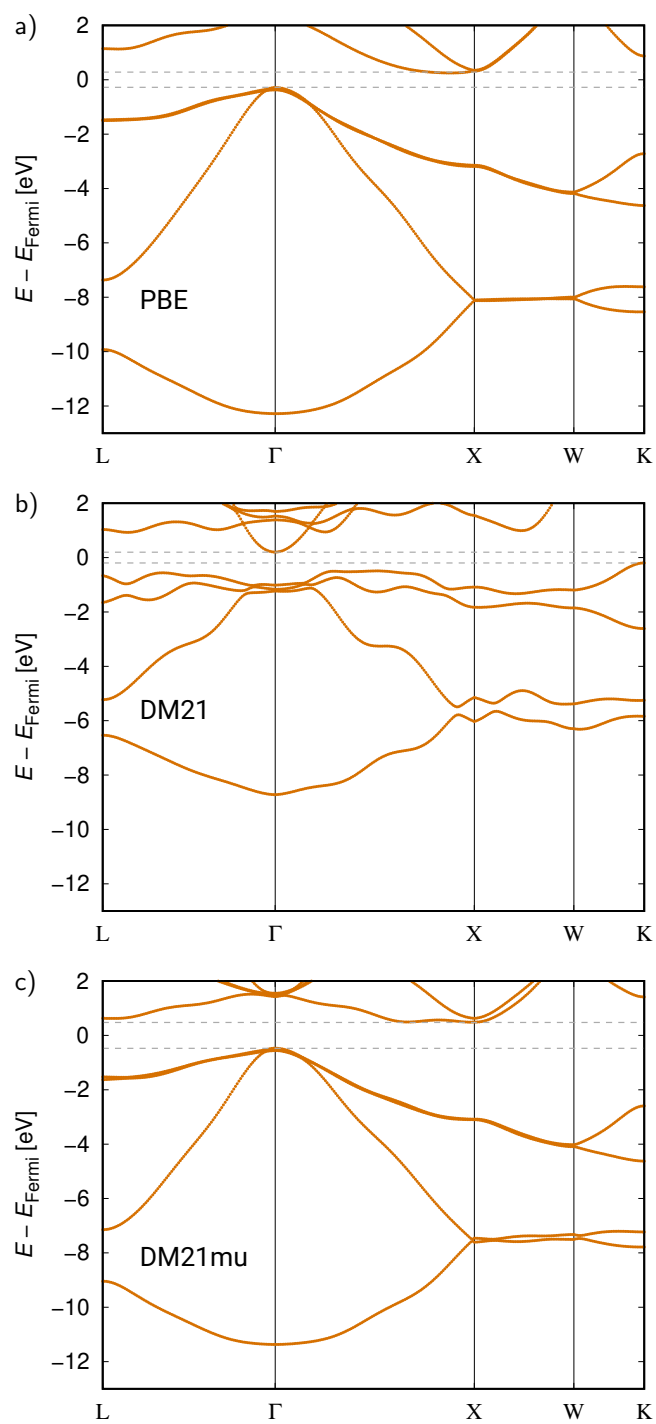


Figure 6: KS bandstructure of Si: a) computed with the PBE functional; b) and c) computed non-selfconsistently using PBE KS orbitals with the DM21 and DM21mu functionals, respectively. The dashed lines indicate the valence and conduction band edges. While PBE and DM21 significantly underestimate the Si band gap, DM21mu yields a good result of ~ 1 eV.

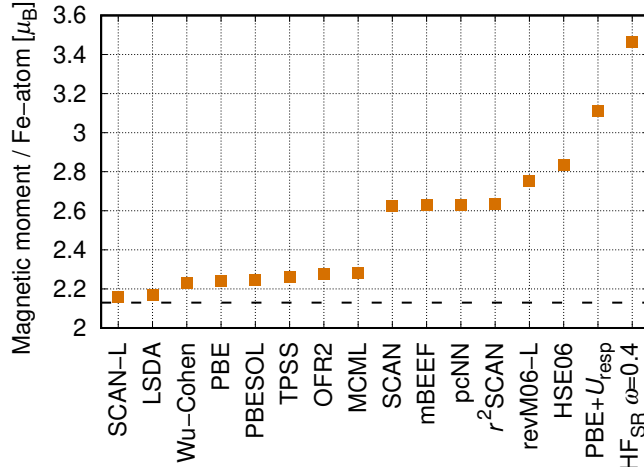


Figure 7: Magnetic moment per primitive body-centered cubic unit cell of bulk Fe obtained with different DFAs: SCAN-L,¹⁹⁸ LSDA,²⁷ Wu-Cohen,³⁰ PBE,¹⁰¹ PBESol,²⁹ TPSS,³³ OFR2,³⁸ MCML,³⁷ SCAN,³⁴ mBEEF,¹³³ pcNN,¹⁴⁴ r^2 SCAN,¹⁹⁹ revM06-L,³⁵ and HSE06.²⁰⁰ PBE+ U_{resp} result with first-principles Hubbard parameter from linear response from Ref. [58]. HF_{SR} $\omega=0.4$ is short-range screened exchange with the same inverse screening length of 0.4/Bohr as for long-range screened exchange used as input feature in the DM21 functionals. The dashed line indicates an experimental value of 2.13 μ_B .²⁰¹

tance of physical constraints on the ML XC models: although DM21mu was only trained on molecular systems, the homogeneous electron gas constraint seems to have extended the range of applicability over DM21 significantly.

It is interesting to note that DM21mu reduces the *sp*-bandwidth of Si compared to PBE. DFAs have a general problem of overestimating bandwidths.¹⁹⁷ Using bandstructures determined from angle-resolved photoemission spectra as accurate training data for ML DFAs could be an option to incorporate the underlying many-body effects into the XC functional (if one chooses to interpret the KS eigenlevels as quasi-particle energies). If DM21mu is transferable to semiconductors in general, will need to be tested on more systems. Extending training data to *GW* quasi-particle bandstructures could be of help to teach the functional derivative discontinuities explicitly for solids (and this would likely cure minor flaws in the DM21mu Si bandstructure such as the lowered conduction band at the L-point).

With these very encouraging results for DM21mu for a semiconductor bandstructure, we now turn to a problem where beyond semi-local DFT approaches typically perform worse than the LDA and GGAs: itinerant ferromagnetism. Figure 7 shows the magnetic moment of bulk Fe computed with a number of different analytical, semi-empirical, and ML DFAs and beyond semi-local DFT methods. Unfortunately, the majority of advanced XC functionals shown here are not able to reproduce the metallic screening of exchange sufficiently and correspondingly yield too large magnetic moments. This problem was addressed in the strongly constrained SCAN functional by deorbitalization:²⁰² the KS kinetic energy dependence was replaced by a density functional for the kinetic energy involving the Laplacian of the charge density, and the resulting SCAN-L¹⁹⁸ and OFR2³⁸ show significantly improved magnetic moments, albeit at the prize of sacrificing constraint fulfillment. Unfortunately,

higher rungs of theory such as the short-range screened hybrid HSE06²⁰⁰ do not lead to an improved description here. Employing a Hubbard- U term to compensate the spurious GGA curvature for fractional electron count even increases the magnetic moment further. Finally, we computed the Fe magnetic moment with short-range screened HF with the same screening length used for long-range screened EXX in the DM21 and DM21mu features, leading to largely exaggerated magnetic moments. Unfortunately, both DM21 and DM21mu show such exaggeratedly large magnetic moments, too (roughly estimated from differences in the spin densities of states computed non-selfconsistently with PBE KS orbitals).

The description of molecular chemistry, correlations due to strongly localized states and metallic screening and delocalized states within the same electronic structure approach is an inherently difficult problem (and a very important one, given the technological importance of interfaces between oxides and metals and their defect chemistries and heterogeneous catalysis). Since imposing analytical constraints and higher levels of theory in semi-local DFT and hybrid DFT turn out to worsen the description of metallic screening, a successful XC approximation is likely going to be a highly nonlocal one. Given this likely complexity of an accurate XC functional, here is thus an opportunity for ML approaches in developing such needed XC approximations.

A major challenge for extending accurate ML XC models to extended systems and metallic phases in particular is that wave-function methods will generally not be applicable. While there is progress in advanced electronic structure methods for solids,²⁰³⁻²⁰⁵ extending approaches to also yield accurate densities important for XC model development, once sufficient accuracy will be reached for energetics leading to a range of training data, will be a major challenge in itself.

9 METHODS

The presented ML DFA benchmarks in the previous section were computed with the following tools. XC energies for hydrogenic ions were evaluated on their analytical nonrelativistic densities through numerical quadrature via SciPy.²⁰⁶ Charge density and KS orbitals for bulk Si were computed using the Quantum Espresso plane-wave DFT code,²⁰⁷ with a plane-wave cut-off of 600 eV and $16 \times 16 \times 16$ k -points sampling the first Brillouin zone. Si ionic cores were described by an SG15 optimized norm-conserving Vanderbilt pseudopotential.^{208,209} Spin density and KS orbitals of bulk Fe were computed with the Vienna Ab initio Simulation Package²¹⁰ with a 500 eV plane-wave cut-off and $28 \times 28 \times 28$ k -points sampling the first Brillouin zone. Fe ionic cores were described by a projector-augmented wave²¹¹ (PAW) potential.²¹² An additional PBE calculation of bulk Fe was performed using Quantum Espresso and a higher plane-wave cut-off of 600 eV and a norm-conserving SG15 pseudopotential, to avoid having to compute PAW augmentation terms in the evaluation of DM21 and DM21mu. DM21 and DM21mu ML XC functionals were evaluated using the C++ interface provided at [213]. The corresponding bandstructure calculations were performed non-selfconsistently with charge density and KS kinetic, EXX, and long-range screened EXX energy densities evaluated with PBE KS orbitals. The zero-wave vector divergence of the Coulomb potential for the EXX computations was treated using the method due to Gygi and Baldereschi.²¹⁴ Band dispersion plots were interpolated with the Wannier90 code.²¹⁵

10 SUMMARY

Quantum chemistry benchmarks and advances in ML approximations to electronic XC enable the development of DFAs targeting chemical accuracy for a range of molecular chemistries. With semi- and nonlocal charge and energy density inputs, ML XC models can be constructed correcting for fundamental limitations of existing DFAs. A challenge for developing chemically accurate ML models for extended systems is the computation of accurate training benchmark energies and densities for these systems. Transferability issues to systems outside the training and validation data are a general concern. Putting these new ML XC developments to the test by the computational chemistry research community will reveal the strengths of these methods and where further development and training data are required.

ACKNOWLEDGMENTS

Support from the U.S. Department of Energy, Office of Science, Office of Basic Energy Sciences, Chemical Sciences, Geosciences, and Biosciences Division, Catalysis Science Program to the SUNCAT Center for Interface Science and Catalysis is gratefully acknowledged.

REFERENCES

1. Keith, J. A.; Vassilev-Galindo, V.; Cheng, B.; Chmiela, S.; Gastegger, M.; Müller, K.-R.; Tkatchenko, A. *Chem. Rev.* **2021**, *121*, 9816–9872.
2. Schmidt, J.; Marques, M. R. G.; Botti, S.; Marques, M. A. L. *npj Comput. Mater.* **2019**, *5*, 83.
3. Von Lilienfeld, O. A.; Burke, K. *Nat. Commun.* **2020**, *11*, 4895.
4. Behler, J.; Parrinello, M. *Phys. Rev. Lett.* **2007**, *98*, 146401.
5. Schütt, K. T.; Saucedo, H. E.; Kindermans, P.-J.; Tkatchenko, A.; Müller, K.-R. *J. Chem. Phys.* **2018**, *148*, 241722.
6. Smith, J. S.; Isayev, O.; Roitberg, A. E. *Chem. Sci.* **2017**, *8*, 3192–3203.
7. Artrith, N.; Urban, A.; Ceder, G. *Phys. Rev. B* **2017**, *96*, 014112.
8. Bartók, A. P.; Payne, M. C.; Kondor, R.; Csányi, G. *Phys. Rev. Lett.* **2010**, *104*, 136403.
9. Chmiela, S.; Tkatchenko, A.; Saucedo, H. E.; Poltavsky, I.; Schütt, K. T.; Müller, K.-R. *Sci. Adv.* **2017**, *3*, e1603015.
10. Unke, O. T.; Chmiela, S.; Saucedo, H. E.; Gastegger, M.; Poltavsky, I.; Schütt, K. T.; Tkatchenko, A.; Müller, K.-R. *Chem. Rev.* **2021**, *121*, 10142–10186.
11. Isayev, O.; Oses, C.; Toher, C.; Gossett, E.; Curtarolo, S.; Tropsha, A. *Nat. Commun.* **2017**, *8*, 15679.
12. Xie, T.; Grossman, J. C. *Phys. Rev. Lett.* **2018**, *120*, 145301.
13. Hautier, G.; Fischer, C. C.; Jain, A.; Mueller, T.; Ceder, G. *Chem. Mater.* **2010**, *22*, 3762–3767.
14. Duvenaud, D. K.; Maclaurin, D.; Iparraguirre, J.; Bombarell, R.; Hirzel, T.; Aspuru-Guzik, A.; Adams, R. P. Convolutional Networks on Graphs for Learning Molecular Fingerprints. *Advances in Neural Information Processing Systems*. 2015; Vol. 28.

15. Ward, L.; Agrawal, A.; Choudhary, A.; Wolverton, C. *npj Comput. Mater.* **2016**, *2*, 16028.
16. Kim, K. et al. *npj Comput. Mater.* **2018**, *4*, 67.
17. Noh, J.; Kim, J.; Stein, H. S.; Sanchez-Lengeling, B.; Gregoire, J. M.; Aspuru-Guzik, A.; Jung, Y. *Matter* **2019**, *1*, 1370–1384.
18. Hohenberg, P.; Kohn, W. *Phys. Rev.* **1964**, *136*, B864.
19. Kohn, W.; Becke, A. D.; Parr, R. G. *J. Phys. Chem.* **1996**, *100*, 12974.
20. Burke, K. *J. Chem. Phys.* **2012**, *136*, 150901.
21. Perdew, J. P.; Ruzsinszky, A.; Constantin, L. A.; Sun, J.; Csonka, G. I. *J. Chem. Theory Comput.* **2009**, *5*, 902–908.
22. Cohen, A. J.; Mori-Sánchez, P.; Yang, W. *Chem. Rev.* **2012**, *112*, 289–320.
23. Becke, A. D. *J. Chem. Phys.* **2014**, *140*, 18A301.
24. Verma, P.; Truhlar, D. G. *Trends Chem.* **2020**, *2*, 302–318.
25. Bryenton, K. R.; Adeleke, A. A.; Dale, S. G.; Johnson, E. R. *WIREs Comput. Mol. Sci.* **2023**, *13*, e1631.
26. Perdew, J. P.; Wang, Y. *Phys. Rev. B* **1992**, *45*, 13244–13249.
27. Perdew, J. P.; Zunger, A. *Phys. Rev. B* **1981**, *23*, 5048–5079.
28. Ceperley, D. M.; Alder, B. J. *Phys. Rev. Lett.* **1980**, *45*, 566–569.
29. Perdew, J. P.; Ruzsinszky, A.; Csonka, G. I.; Vydrov, O. A.; Scuseria, G. E.; Constantin, L. A.; Zhou, X.; Burke, K. *Phys. Rev. Lett.* **2008**, *100*, 136406.
30. Wu, Z.; Cohen, R. E. *Phys. Rev. B* **2006**, *73*, 235116.
31. Zhang, Y.; Yang, W. *Phys. Rev. Lett.* **1998**, *80*, 890.
32. Hammer, B.; Hansen, L. B.; Nørskov, J. K. *Phys. Rev. B* **1999**, *59*, 7413.
33. Tao, J.; Perdew, J. P.; Staroverov, V. N.; Scuseria, G. E. *Phys. Rev. Lett.* **2003**, *91*, 146401.
34. Sun, J.; Ruzsinszky, A.; Perdew, J. P. *Phys. Rev. Lett.* **2015**, *115*, 036402.
35. Wang, Y.; Jin, X.; Yu, H. S.; Truhlar, D. G.; He, X. *Proc. Natl. Acad. Sci.* **2017**, *114*, 8487–8492.
36. Garza, A. J.; Bell, A. T.; Head-Gordon, M. *J. Chem. Theory Comput.* **2018**, *14*, 3083–3090.
37. Brown, K.; Maimaiti, Y.; Trepte, K.; Bligaard, T.; Voss, J. *J. Comput. Chem.* **2021**, *42*, 2004–2013.
38. Kaplan, A. D.; Perdew, J. P. *Phys. Rev. Mater.* **2022**, *6*, 083803.
39. Becke, A. D. *J. Chem. Phys.* **1993**, *98*, 1372–1377.
40. Iikura, H.; Tsuneda, T.; Yanai, T.; Hirao, K. *J. Chem. Phys.* **2001**, *115*, 3540–3544.
41. Leininger, T.; Stoll, H.; Werner, H.-J.; Savin, A. *Chem. Phys. Lett.* **1997**, *275*, 151–160.
42. Heyd, J.; Scuseria, G. E.; Ernzerhof, M. *J. Chem. Phys.* **2003**, *118*, 8207–8215.
43. Mallikarjun Sharada, S.; Karlsson, R. K. B.; Maimaiti, Y.; Voss, J.; Bligaard, T. *Phys. Rev. B* **2019**, *100*, 035439.
44. Vydrov, O. A.; Scuseria, G. E. *J. Chem. Phys.* **2004**, *121*, 8187–8193.
45. Perdew, J. P.; Ruzsinszky, A.; Sun, J.; Pederson, M. R. In *Chapter One - Paradox of Self-Interaction Correction: How Can Anything So Right Be So Wrong?*; Arimondo, E., Lin, C. C., Yelin, S. F., Eds.; Advances In Atomic, Molecular, and Optical Physics; Academic Press, 2015; Vol. 64; pp 1–14.
46. Mayhall, N. J.; Head-Gordon, M. *J. Phys. Chem. Lett.* **2015**, *6*, 1982–1988.

47. Noodleman, L. *J. Chem. Phys.* **1981**, *74*, 5737–5743.
48. Daul, C. *Int. J. Quant. Chem.* **1994**, *52*, 867–877.
49. Bohm, D.; Pines, D. *Phys. Rev.* **1951**, *82*, 625–634.
50. Paier, J.; Janesko, B. G.; Henderson, T. M.; Scuseria, G. E.; Grüneis, A.; Kresse, G. *J. Chem. Phys.* **2010**, *132*, 094103.
51. Perdew, J. P.; Parr, R. G.; Levy, M.; Balduz, J. L. *Phys. Rev. Lett.* **1982**, *49*, 1691–1694.
52. Mori-Sánchez, P.; Cohen, A. J.; Yang, W. *J. Chem. Phys.* **2006**, *125*, 201102.
53. Anisimov, V. I.; Zaanen, J.; Andersen, O. K. *Phys. Rev. B* **1991**, *44*, 943.
54. Czyżyk, M. T.; Sawatzky, G. A. *Phys. Rev. B* **1994**, *49*, 14211.
55. Liechtenstein, A. I.; Anisimov, V. I.; Zaanen, J. *Phys. Rev. B* **1995**, *52*, R5467.
56. Cococcioni, M.; de Gironcoli, S. *Phys. Rev. B* **2005**, *71*, 035105.
57. Wang, L.; Maxisch, T.; Ceder, G. *Phys. Rev. B* **2006**, *73*, 195107.
58. Voss, J. *J. Phys. Commun.* **2022**, *6*, 035009.
59. Mori-Sánchez, P.; Cohen, A. J.; Yang, W. *Phys. Rev. Lett.* **2008**, *100*, 146401.
60. Kuisma, M.; Ojanen, J.; Enkovaara, J.; Rantala, T. T. *Phys. Rev. B* **2010**, *82*, 115106.
61. Andersson, Y.; Langreth, D. C.; Lundqvist, B. I. *Phys. Rev. Lett.* **1996**, *76*, 102–105.
62. Dion, M.; Rydberg, H.; Schröder, E.; Langreth, D. C.; Lundqvist, B. I. *Phys. Rev. Lett.* **2004**, *92*, 246401.
63. Vydrov, O. A.; Van Voorhis, T. *J. Chem. Phys.* **2010**, *133*, 244103.
64. Grimme, S. *J. Comput. Chem.* **2006**, *27*, 1787–1799.
65. Caldeweyher, E.; Ehlert, S.; Hansen, A.; Neugebauer, H.; Spicher, S.; Bannwarth, C.; Grimme, S. *J. Chem. Phys.* **2019**, *150*, 154122.
66. Tkatchenko, A.; Scheffler, M. *Phys. Rev. Lett.* **2009**, *102*, 073005.
67. Sato, T.; Nakai, H. *J. Chem. Phys.* **2009**, *131*, 224104.
68. Steinmann, S. N.; Corminboeuf, C. *J. Chem. Phys.* **2011**, *134*, 044117.
69. Curtiss, L. A.; Raghavachari, K.; Redfern, P. C.; Rassolov, V.; Pople, J. A. *J. Chem. Phys.* **1998**, *109*, 7764–7776.
70. Curtiss, L. A.; Redfern, P. C.; Raghavachari, K. *J. Chem. Phys.* **2007**, *126*, 084108.
71. Curtiss, L. A.; Raghavachari, K.; Redfern, P. C.; Pople, J. A. *J. Chem. Phys.* **2000**, *112*, 7374–7383.
72. Curtiss, L. A.; Redfern, P. C.; Raghavachari, K. *J. Chem. Phys.* **2005**, *123*, 124107.
73. Ramakrishnan, R.; Dral, P. O.; Rupp, M.; Von Lilienfeld, O. A. *Sci. Data* **2014**, *1*, 140022.
74. Curtiss, L. A.; Redfern, P. C.; Raghavachari, K. *J. Chem. Phys.* **2007**, *127*, 124105.
75. Ruddigkeit, L.; van Deursen, R.; Blum, L. C.; Reymond, J.-L. *J. Chem. Inf. Model.* **2012**, *52*, 2864–2875.
76. Karton, A.; Rabinovich, E.; Martin, J. M. L.; Ruscic, B. *J. Chem. Phys.* **2006**, *125*, 144108.
77. Karton, A.; Taylor, P. R.; Martin, J. M. L. *J. Chem. Phys.* **2007**, *127*, 064104.
78. Karton, A.; Daon, S.; Martin, J. M. L. *Chem. Phys. Lett.* **2011**, *510*, 165–178.
79. Karton, A.; Sylvetsky, N.; Martin, J. M. L. *J. Comput. Chem.* **2017**, *38*, 2063–2075.
80. Řezáč, J.; Riley, K. E.; Hobza, P. *J. Chem. Theory Comput.* **2011**, *7*, 2427–2438.
81. Řezáč, J.; Riley, K. E.; Hobza, P. *J. Chem. Theory Comput.* **2011**, *7*, 3466–3470.
82. Čížek, J. *J. Chem. Phys.* **1966**, *45*, 4256–4266.

83. Brauer, B.; Kesharwani, M. K.; Kozuch, S.; Martin, J. M. L. *Phys. Chem. Chem. Phys.* **2016**, *18*, 20905–20925.
84. Zheng, J.; Zhao, Y.; Truhlar, D. G. *J. Chem. Theory Comput.* **2007**, *3*, 569–582.
85. Zheng, J.; Zhao, Y.; Truhlar, D. G. *J. Chem. Theory Comput.* **2009**, *5*, 808–821.
86. Zhao, Y.; Lynch, B. J.; Truhlar, D. G. *J. Phys. Chem. A* **2004**, *108*, 2715–2719.
87. Zhao, Y.; González-García, N.; Truhlar, D. G. *J. Phys. Chem. A* **2005**, *109*, 2012–2018.
88. Goerigk, L.; Hansen, A.; Bauer, C.; Ehrlich, S.; Najibi, A.; Grimme, S. *Phys. Chem. Chem. Phys.* **2017**, *19*, 32184–32215.
89. Mardirossian, N.; Head-Gordon, M. *Mol. Phys.* **2017**, *115*, 2315–2372.
90. Chan, B.; Gill, P. M. W.; Kimura, M. *J. Chem. Theory Comput.* **2019**, *15*, 3610–3622.
91. Kubaschewski, O.; Spencer, P. J.; Alcock, C. B. *Materials thermochemistry*, 6th ed.; Pergamon Press: Oxford, 1993.
92. Jain, A.; Hautier, G.; Ong, S. P.; Moore, C. J.; Fischer, C. C.; Persson, K. A.; Ceder, G. *Phys. Rev. B* **2011**, *84*, 045115.
93. Jain, A.; Ong, S. P.; Hautier, G.; Chen, W.; Richards, W. D.; Dacek, S.; Cholia, S.; Gunter, D.; Skinner, D.; Ceder, G.; Persson, K. A. *APL Mater.* **2013**, *1*, 011002.
94. Kirklin, S.; Saal, J. E.; Meredig, B.; Thompson, A.; Doak, J. W.; Aykol, M.; Rühl, S.; Wolverton, C. *npj Comput. Mater.* **2015**, *1*, 15010.
95. Lundgaard, K. T.; Wellendorff, J.; Voss, J.; Jacobsen, K. W.; Bligaard, T. *Phys. Rev. B* **2016**, *93*, 235162.
96. Zhang, G.-X.; Reilly, A. M.; Tkatchenko, A.; Scheffler, M. *New J. Phys.* **2018**, *20*, 063020.
97. Staroverov, V. N.; Scuseria, G. E.; Tao, J.; Perdew, J. P. *J. Chem. Phys.* **2003**, *119*, 12129–12137.
98. Curtiss, L. A.; Redfern, P. C.; Raghavachari, K.; Pople, J. A. *J. Chem. Phys.* **2001**, *114*, 108–117.
99. Alchagirov, A. B.; Perdew, J. P.; Boettger, J. C.; Albers, R. C.; Fiolhais, C. *Phys. Rev. B* **2001**, *63*, 224115.
100. Hao, P.; Fang, Y.; Sun, J.; Csonka, G. I.; Philippsen, P. H. T.; Perdew, J. P. *Phys. Rev. B* **2012**, *85*, 014111.
101. Perdew, J. P.; Burke, K.; Ernzerhof, M. *Phys. Rev. Lett.* **1996**, *77*, 3865.
102. Trepte, K.; Voss, J. *J. Comput. Chem.* **2022**, *43*, 1104–1112.
103. Wellendorff, J.; Silbaugh, T. L.; Garcia-Pintos, D.; Nørskov, J. K.; Bligaard, T.; Studt, F.; Campbell, C. T. *Surface Science* **2015**, *640*, 36–44.
104. Mallikarjun Sharada, S.; Bligaard, T.; Luntz, A. C.; Kroes, G.-J.; Nørskov, J. K. *J. Phys. Chem. C* **2017**, *121*, 19807–19815.
105. Tchakoua, T.; Gerrits, N.; Smeets, E. W. F.; Kroes, G.-J. *J. Chem. Theory Comput.* **2023**, *19*, 245–270.
106. Medvedev, M. G.; Bushmarinov, I. S.; Sun, J.; Perdew, J. P.; Lyssenko, K. A. *Science* **2017**, *355*, 49–52.
107. LeCun, Y.; Bengio, Y.; Hinton, G. *Nature* **2015**, *521*, 436–444.
108. Becke, A. D. *J. Chem. Phys.* **1993**, *98*, 5648–5652.
109. Curtiss, L. A.; Raghavachari, K.; Trucks, G. W.; Pople, J. A. *J. Chem. Phys.* **1991**, *94*, 7221–7230.

110. Perdew, J. P. In *Unified Theory of Exchange and Correlation Beyond the Local Density Approximation, Electronic Structure of Solids '91*; Ziesche, P., Eschrig, H., Eds.; Akademie Verlag: Berlin, 1991; p 11.
111. Lee, C.; Yang, W.; Parr, R. G. *Phys. Rev. B* **1988**, *37*, 785–789.
112. Stephens, P. J.; Devlin, F. J.; Chabalowski, C. F.; Frisch, M. J. *J. Phys. Chem.* **1994**, *98*, 11623–11627.
113. Vargas-Hernández, R. A. *J. Phys. Chem. A* **2020**, *124*, 4053–4061.
114. Mockus, J. *Bayesian approach to global optimization: theory and applications*; Mathematics and its applications Soviet series 37; Kluwer Acad. Publ: Dordrecht, 1989.
115. Becke, A. D. *J. Chem. Phys.* **1997**, *107*, 8554–8560.
116. Mardirossian, N.; Head-Gordon, M. *Phys. Chem. Chem. Phys.* **2014**, *16*, 9904.
117. Liu, Y.; Zhang, C.; Liu, Z.; Truhlar, D. G.; Wang, Y.; He, X. *Nat Comput Sci* **2022**, *3*, 48–58.
118. Hamprecht, F. A.; Cohen, A. J.; Tozer, D. J.; Handy, N. C. *J. Chem. Phys.* **1998**, *109*, 6264–6271.
119. Boese, A. D.; Doltsinis, N. L.; Handy, N. C.; Sprik, M. *J. Chem. Phys.* **2000**, *112*, 1670–1678.
120. Menconi, G.; Wilson, P. J.; Tozer, D. J. *J. Chem. Phys.* **2001**, *114*, 3958–3967.
121. Boese, A. D.; Chandra, A.; Martin, J. M. L.; Marx, D. *J. Chem. Phys.* **2003**, *119*, 5965–5980.
122. Zhao, Y.; Schultz, N. E.; Truhlar, D. G. *J. Chem. Phys.* **2005**, *123*, 161103.
123. Zhao, Y.; Truhlar, D. G. *J. Chem. Phys.* **2006**, *125*, 194101.
124. Zhao, Y.; Truhlar, D. G. *Theor. Chem. Account.* **2008**, *120*, 215–241.
125. Peverati, R.; Truhlar, D. G. *J. Phys. Chem. Lett.* **2012**, *3*, 117–124.
126. Yu, H. S.; He, X.; Truhlar, D. G. *J. Chem. Theory Comput.* **2016**, *12*, 1280–1293.
127. Wang, Y.; Verma, P.; Zhang, L.; Li, Y.; Liu, Z.; Truhlar, D. G.; He, X. *Proc. Natl. Acad. Sci.* **2020**, *117*, 2294–2301.
128. Zhao, Y.; Schultz, N. E.; Truhlar, D. G. *J. Chem. Theory Comput.* **2006**, *2*, 364–382.
129. Perdew, J. P.; Ruzsinszky, A.; Sun, J.; Burke, K. *J. Chem. Phys.* **2014**, *140*, 18A533.
130. Kaplan, A. D.; Levy, M.; Perdew, J. P. *Annu. Rev. Phys. Chem.* **2023**, *74*, 193–218.
131. Sparrow, Z. M.; Ernst, B. G.; Quady, T. K.; DiStasio, R. A. J. *J. Phys. Chem. Lett.* **2022**, *13*, 6896–6904.
132. N., T. A. *Sov. Math. Dok.* **1963**, *4*, 1035–1038.
133. Wellendorff, J.; Lundgaard, K. T.; Jacobsen, K. W.; Bligaard, T. *J. Chem. Phys.* **2014**, *140*, 144107.
134. Wellendorff, J.; Lundgaard, K. T.; Møgelhøj, A.; Petzold, V.; Landis, D. D.; Nørskov, J. K.; Bligaard, T.; Jacobsen, K. W. *Phys. Rev. B* **2012**, *85*, 235149.
135. Hoerl, A. E.; Kennard, R. W. *Technometrics* **1970**, *12*, 55–67.
136. Kovács, P.; Tran, F.; Blaha, P.; Madsen, G. K. H. *J. Chem. Phys.* **2022**, *157*, 094110.
137. Gastegger, M.; González, L.; Marquetand, P. *Monatsh. Chem.* **2019**, *150*, 173–182.
138. Koza, J. *Stat. Comput.* **1994**, *4*, 87–112.
139. Ma, H.; Narayanaswamy, A.; Riley, P.; Li, L. *Sci. Adv.* **2022**, *8*, eabq0279.
140. Real, E.; Aggarwal, A.; Huang, Y.; Le, Q. V. *AAAI* **2019**, *33*, 4780–4789.
141. Riemelmoser, S.; Verdi, C.; Kaltak, M.; Kresse, G. *J. Chem. Theory Comput.* **2023**, *19*, 7287–7299.

142. Rumelhart, D. E.; Hinton, G. E.; Williams, R. J. *Nature* **1986**, *323*, 533–536.
143. Nagai, R.; Akashi, R.; Sugino, O. *npj Comput. Mater.* **2020**, *6*, 43.
144. Nagai, R.; Akashi, R.; Sugino, O. *Phys. Rev. Res.* **2022**, *4*, 013106.
145. Kirkpatrick, J. et al. *Science* **2021**, *374*, 1385–1389.
146. Wu, Q.; Yang, W. *J. Chem. Phys.* **2003**, *118*, 2498–2509.
147. Gedeon, J.; Schmidt, J.; Hodgson, M. J. P.; Wetherell, J.; Benavides-Riveros, C. L.; Marques, M. A. L. *Mach. Learn.: Sci. Technol.* **2022**, *3*, 015011.
148. Wang, J.; Wang, Y.; Xu, R.-X.; Chen, G.; Zheng, X. *J. Chem. Phys.* **2023**, *158*, 154107.
149. Chen, Y.; Zhang, L.; Wang, H.; E, W. *J. Chem. Theory Comput.* **2021**, *17*, 170–181.
150. Li, L.; Hoyer, S.; Pederson, R.; Sun, R.; Cubuk, E. D.; Riley, P.; Burke, K. *Phys. Rev. Lett.* **2021**, *126*, 036401.
151. White, S. R. *Phys. Rev. Lett.* **1992**, *69*, 2863–2866.
152. Kalita, B.; Pederson, R.; Chen, J.; Li, L.; Burke, K. *J. Phys. Chem. Lett.* **2022**, *13*, 2540–2547.
153. Kasim, M.; Vinko, S. *Phys. Rev. Lett.* **2021**, *127*, 126403.
154. Kasim, M. F.; Lehtola, S.; Vinko, S. M. *J. Chem. Phys.* **2022**, *156*, 084801.
155. Tozer, D. J.; Ingamells, V. E.; Handy, N. C. *J. Chem. Phys.* **1996**, *105*, 9200–9213.
156. Zhao, Q.; Morrison, R. C.; Parr, R. G. *Phys. Rev. A* **1994**, *50*, 2138–2142.
157. Breiman, L. *Neural Comput.* **1999**, *11*, 1493–1517.
158. Friedman, J. H. *Ann. Stat.* **2001**, *29*, 1189–1232.
159. Wang, J.; Zhang, D.; Xu, R.-X.; Yam, C.; Chen, G.; Zheng, X. *J. Phys. Chem. A* **2022**, *126*, 970–978.
160. Chen, T.; Guestrin, C. XGBoost: A Scalable Tree Boosting System. Proceedings of the 22nd ACM SIGKDD International Conference on Knowledge Discovery and Data Mining. San Francisco, CA, 2016; pp 785–794.
161. Bogojeski, M.; Vogt-Maranto, L.; Tuckerman, M. E.; Müller, K.-R.; Burke, K. *Nat. Commun.* **2020**, *11*, 5223.
162. Margraf, J. T.; Reuter, K. *Nat. Commun.* **2021**, *12*, 344.
163. Chen, Y.; Zhang, L.; Wang, H.; E, W. *J. Phys. Chem. A* **2020**, *124*, 7155–7165.
164. Cheng, L.; Welborn, M.; Christensen, A. S.; Miller, T. F. *J. Chem. Phys.* **2019**, *150*, 131103.
165. Rasmussen, C. E.; Williams, C. K. I. *Gaussian processes for machine learning*; Adaptive computation and machine learning; MIT Press: Cambridge, MA, 2006.
166. Ng, W.-P.; Liang, Q.; Yang, J. *J. Chem. Theory Comput.* **2023**, *19*, 5439–5449.
167. Han, R.; Rodríguez-Mayorga, M.; Lubner, S. *J. Chem. Theory Comput.* **2021**, *17*, 777–790.
168. Møller, C.; Plesset, M. S. *Phys. Rev.* **1934**, *46*, 618–622.
169. Ramakrishnan, R.; Dral, P. O.; Rupp, M.; Von Lilienfeld, O. A. *J. Chem. Theory Comput.* **2015**, *11*, 2087–2096.
170. Proppe, J.; Gugler, S.; Reiher, M. *J. Chem. Theory Comput.* **2019**, *15*, 6046–6060.
171. Dick, S.; Fernandez-Serra, M. *J. Chem. Phys.* **2019**, *151*, 144102.
172. Babin, V.; Leforestier, C.; Paesani, F. *J. Chem. Theory Comput.* **2013**, *9*, 5395–5403.
173. Babin, V.; Medders, G. R.; Paesani, F. *J. Chem. Theory Comput.* **2014**, *10*, 1599–1607.
174. Dick, S.; Fernandez-Serra, M. *Nat. Commun.* **2020**, *11*, 3509.

175. Snyder, J. C.; Rupp, M.; Hansen, K.; Müller, K.-R.; Burke, K. *Phys. Rev. Lett.* **2012**, *108*, 253002.
176. Li, L.; Snyder, J. C.; Pelaschier, I. M.; Huang, J.; Niranjana, U.; Duncan, P.; Rupp, M.; Müller, K.; Burke, K. *Int. J. Quant. Chem.* **2016**, *116*, 819–833.
177. Tan, C. W.; Pickard, C. J.; Witt, W. C. *J. Chem. Phys.* **2023**, *158*, 124801.
178. Brockherde, F.; Vogt, L.; Li, L.; Tuckerman, M. E.; Burke, K.; Müller, K.-R. *Nat. Commun.* **2017**, *8*, 872.
179. Grisafi, A.; Fabrizio, A.; Meyer, B.; Wilkins, D. M.; Corminboeuf, C.; Ceriotti, M. *ACS Cent. Sci.* **2019**, *5*, 57–64.
180. Fabrizio, A.; Grisafi, A.; Meyer, B.; Ceriotti, M.; Corminboeuf, C. *Chem. Sci.* **2019**, *10*, 9424–9432.
181. Chandrasekaran, A.; Kamal, D.; Batra, R.; Kim, C.; Chen, L.; Ramprasad, R. *npj Comput Mater* **2019**, *5*, 22.
182. Zepeda-Núñez, L.; Chen, Y.; Zhang, J.; Jia, W.; Zhang, L.; Lin, L. *J. Comp. Phys.* **2021**, *443*, 110523.
183. Del Rio, B. G.; Phan, B.; Ramprasad, R. *npj Comput. Mater.* **2023**, *9*, 158.
184. Focassio, B.; Domina, M.; Patil, U.; Fazzio, A.; Sanvito, S. *npj Comput. Mater.* **2023**, *9*, 87.
185. Shao, X.; Paetow, L.; Tuckerman, M. E.; Pavanello, M. *Nat Commun* **2023**, *14*, 6281.
186. Cuierrier, E.; Roy, P.-O.; Wang, R.; Ernzerhof, M. *J. Chem. Phys.* **2022**, *157*, 171103.
187. Wang, R.; Zhou, Y.; Ernzerhof, M. *Phys. Rev. A* **2017**, *96*, 022502.
188. Lei, X.; Medford, A. J. *Phys. Rev. Mater.* **2019**, *3*, 063801.
189. Yu, M.; Yang, S.; Wu, C.; Marom, N. *npj Comput. Mater.* **2020**, *6*, 180.
190. Bystrom, K.; Kozinsky, B. *J. Chem. Theory Comput.* **2022**, *18*, 2180–2192.
191. Gunnarsson, O.; Lundqvist, B. I. *Phys. Rev. B* **1976**, *13*, 4274–4298.
192. Perdew, J. P. *Phys. Rev. Lett.* **1985**, *55*, 1665–1668.
193. Becke, A. D. *J. Chem. Phys.* **2022**, *156*, 214101.
194. Hammes-Schiffer, S. *Science* **2017**, *355*, 28–29.
195. Hedin, L. *Phys. Rev.* **1965**, *139*, A796–A823.
196. Hybertsen, M. S.; Louie, S. G. *Phys. Rev. B* **1986**, *34*, 5390–5413.
197. Northrup, J. E.; Hybertsen, M. S.; Louie, S. G. *Phys. Rev. Lett.* **1987**, *59*, 819–822.
198. Mejía-Rodríguez, D.; Trickey, S. B. *Phys. Rev. B* **2018**, *98*, 115161.
199. Furness, J. W.; Kaplan, A. D.; Ning, J.; Perdew, J. P.; Sun, J. *J. Phys. Chem. Lett.* **2020**, *11*, 8208–8215.
200. Heyd, J.; Scuseria, G. E.; Ernzerhof, M. *J. Chem. Phys.* **2006**, *124*, 219906.
201. Wijn, H. P. J. In *3d, 4d and 5d Elements, Alloys and Compounds*; Wijn, H. P. J., Ed.; Springer: Berlin/Heidelberg, 1997; Vol. 32A; pp 40–45, Series Title: Landolt-Börnstein - Group III Condensed Matter.
202. Mejía-Rodríguez, D.; Trickey, S. B. *Phys. Rev. B* **2019**, *100*, 041113.
203. Olsen, T.; Patrick, C. E.; Bates, J. E.; Ruzsinszky, A.; Thygesen, K. S. *npj Comput. Mater.* **2019**, *5*, 106.
204. Kent, P. R. C. et al. *J. Chem. Phys.* **2020**, *152*, 174105.
205. Cassella, G.; Sutterud, H.; Azadi, S.; Drummond, N. D.; Pfau, D.; Spencer, J. S.; Foulkes, W. M. C. *Phys. Rev. Lett.* **2023**, *130*, 036401.
206. Virtanen, P. et al. *Nat. Methods* **2020**, *17*, 261.

207. Giannozzi, P. et al. *J. Phys.: Condens. Matter* **2009**, *21*, 395502.
208. Hamann, D. R. *Phys. Rev. B* **2013**, *88*, 085117.
209. Schlipf, M.; Gygi, F. *Comp. Phys. Commun.* **2015**, *196*, 36–44.
210. Kresse, G.; Furthmüller, J. *Phys. Rev. B* **1993**, *54*, 11169.
211. Blöchl, P. E. *Phys. Rev. B* **1994**, *50*, 17953–17979.
212. Kresse, G.; Joubert, D. *Phys. Rev. B* **1999**, *59*, 1758.
213. https://github.com/google-deepmind/deepmind-research/tree/master/density_functional_approximation_dm21#using-dm21-from-c
(visited 08/21/2023).
214. Gygi, F.; Baldereschi, A. *Phys. Rev. B* **1986**, *34*, 4405–4408.
215. Pizzi, G. et al. *J. Phys.: Condens. Matter* **2020**, *32*, 165902.